Applied Catalysis B: Environmental 258 (2019) 117985

Contents lists available at ScienceDirect

Applied Catalysis B: Environmental

journal homepage: www.elsevier.com/locate/apcatb

Revealing the active species of Cu-based catalysts for heterogeneous Fenton reaction

Yang Sun[a], Pengfei Tian[a], Doudou Ding[a], Zixu Yang[a], Weizhi Wang[a], Hui Xin[a], Jing Xu[a], Yi-Fan Han[a,b,*]

[a] State Key Laboratory of Chemical Engineering, East China University of Science and Technology, Shanghai 200237, China
[b] Research Center of Heterogeneous Catalysis and Engineering Sciences, School of Chemical Engineering and Energy, Zhengzhou University, Zhengzhou 450001, China

ARTICLE INFO

Keywords:
Active species
Cu-based catalysts
Heterogeneous fenton
Structure-performance relationship

ABSTRACT

Cu-based heterogeneous Fenton catalysts are promising for industrial wastewater treatment, nevertheless it remains a great challenge to understand the catalytic mechanism due to the difficulty in identifying the critical roles of coexisting Cu^0, Cu^+ and Cu^{2+} species in the technical catalysts. In order to identify the catalytic roles of various copper species, core-shell $Cu@SiO_2$ catalysts reduced at different reduction temperatures were studied for rhodamine B degradation. The Cu^+ dominating catalyst, $Cu@SiO_2$-R200, exhibited the highest degradation rate with more than 95% RhB (10 ppm) removal within 10 min. Combined with multiple techniques, including in situ spectroscopy, and density functional theory calculations, it can be concluded that Cu^+ acts as the primary active species with the highest efficiency in activating the H_2O_2 to produce ·OH and subsequently degrading the contaminants. In this work, the structure-performance relationship of Cu-based heterogeneous Fenton reaction was elucidated to inspire the rational design of high-performance heterogeneous catalysts.

1. Introduction

Fenton reaction, which can generate strong oxidative hydroxyl radicals (·OH), is attracting increasing attention due to its high capacity for the degradation of organic contaminants which are not biodegradable [1–4]. Comparing with the conventional homogeneous Fenton reaction (Fe^{2+}/H_2O_2), the Cu-based heterogeneous Fenton process is more advantageous for practical application due to the avoidance of producing large amount of undesired iron sludge in the effluent, facile separation of the catalyst and broad operation pH range [5]. Copper nanoparticles, either in bulk form or incorporated into various supports (i.e. Al_2O_3, SiO_2, TiO_2 and zeolites) have already been reported to be effective on the removal of various organic pollutants such as phenol, phenytoin, ibuprofen, diphenhydramine, bisphenol A, benzoic acid, nitrobenzene and diethyl phthalate [5–13]. Particularly, our recent work [14] found that Cu-Fe bimetallic catalysts demonstrated high catalytic performance for the degradation of nitrobenzene, and doping Cu to Fe-based catalysts markedly prohibited the generation of the highly toxic intermediate 1,3-dinitrobezene.

Although Cu-based Fenton catalysts have been extensively studied [15–17], it is still a challenge to identify the active Cu species for Fenton reaction and to further unravel the catalytic mechanism and structure-performance relationship of the catalyst, since Cu^0, Cu^+ and Cu^{2+} species always coexist in technical catalysts; nevertheless, the exact role of each Cu species in the catalytic reaction remains ambiguous. Most studies have simply assumed that Cu-based heterogeneous Fenton catalysts share the same catalytic mechanism as homogeneous Cu catalysts [7,18], which proposed that Cu^+ or its complexes activated H_2O_2 to produce ·OH and was oxidized to Cu^{2+} simultaneously [15,19,20]. Moreover, many researchers who studied zero valent copper (ZVC) catalysts proposed that ·OH could be generated through the catalytic decomposition of H_2O_2 over homogeneous Cu^+ due to the corrosive dissolution in the suspension [12,21].

Nevertheless, all of the abovementioned catalytic mechanisms follow the homogeneous mechanism, which cannot properly elucidate the heterogeneous Fenton reaction. Two critical aspects are different between the heterogeneous and homogeneous Fenton processes: (1) the adsorption of reactants and the desorption of products on the catalyst surface are necessary for the former, while there are no such steps in the latter; (2) the heterogeneous catalytic reaction takes place on the catalyst surface, whereas the homogeneous reaction proceeds in the solution.

To date, no mechanism with concrete experimental evidences has been available for the heterogeneous Fenton reaction. The major

* Corresponding author.
E-mail address: yifanhan@ecust.edu.cn (Y.-F. Han).

https://doi.org/10.1016/j.apcatb.2019.117985
Received 10 June 2019; Received in revised form 19 July 2019; Accepted 21 July 2019
Available online 23 July 2019
0926-3373/

challenge is that the active copper species is difficult to control during the catalyst preparation. Particularly, as a high-energy species [22,23], Cu^+ is highly unstable in conventional supported Cu catalysts. In order to figure out the roles of various copper species in the heterogeneous Fenton reaction, Cu NPs with different dominant Cu species, or to say, structure-control catalysts, are meaningful to the study of the origin of active sites on solid catalysts.

Recently, active metal NPs encapsulated in porous shells with high thermal and chemical stabilities during the reaction process have been reported. A Pt@mSiO_2 catalyst with high-temperature stability was reported to overcome the drawback of low activity for Pt@Co core-shell catalyst [24,25]. In addition, by embedding Cu nanoparticles in mesoporous silica shells, highly stable Cu catalysts with controllable concentration of Cu^0 and Cu^+ were prepared for dehydrogenation of methanol to methyl formate [26]. Inspired by the idea of core-shell structure, we prepare a CuO core-silica shell (designated as Cu@SiO_2) structure with tunable active species on the loaded copper NPs.

Herein, Cu@SiO_2 catalysts were evaluated in the case of degrading rhodamine B (RhB) and other organic pollutants. High catalytic performance was observed by reducing the catalyst in a H_2 flow at 200 °C. The catalytic roles of Cu^0, Cu^+ and Cu^{2+} and the structure-performance relationship of Cu-based heterogeneous Fenton catalysts were fully clarified by employing density functional theory (DFT) calculations and multiple characterizations including in situ diffuse reflectance infrared Fourier transform spectroscopy of CO adsorption (CO-DRIFTS), X-ray photoelectron spectroscopy (XPS) and X-ray absorption near-edge structure spectra (XANES). This study proposed possible catalytic mechanism of the Cu-based heterogeneous Fenton catalysts based on elucidating the roles of various copper species during reaction. The findings from this study are expected to provide new insights to advance the current Fenton process.

2. Experimental

2.1. Catalyst preparation

Cu@SiO_2 catalysts were prepared via a procedure reported by Yang et al. with a minor modification [26]. Firstly, 7.25 g polyvinylpyrrolidone (PVP) and 1.80 g $Cu(NO_3)_2{\cdot}3H_2O$ were dissolved in 1000 mL ethanol to form the precursor solution. Then, the precursor solution was precipitated by a mixed solution of 3 g of cetyltrimethyl ammonium bromide (CTAB), 144 mL of ammonia (28%), 1028 mL of ethanol and 818 mL of water. When the deep blue transparent solution was formed, 50 mL of tetraethoxysilane (TEOS) ethanol solution (V_{TEOS} / $V_{ethanol}$ = 0.25) was added dropwise (0.5 mL/min) and stirred for 48 h. The resultant solid was collected by centrifugation and washed with distilled water and ethanol. After being dried at 80 °C for 12 h and calcined at 550 °C for 6 h, the Cu@SiO_2 was obtained. In the reduction process, the catalyst was subjected to reduction at setting temperatures (T) in 10% H_2/Ar for 2 h at a ramping rate of 2 °C/min. The as-prepared catalysts were donated as Cu@SiO_2-R(T).

2.2. Characterization

The crystal structures of the prepared catalysts were determined with a Bruker D8-Advance X-ray powder diffractometer with a Cu Kα ray source (λ = 0.154 nm) at 40 kV and 40 mA. The data were collected in a step-scan mode within the range of 5–80° (2θ) with an interval of 0.02°.

Transmission electron microscopy (TEM) and high-angle annular dark-field scanning transmission electron microscopy (HAADF-STEM) images of the synthesized catalysts were recorded on JEOL 2100 and HT7700 microscopes, respectively, and the samples were prepared by a resin embedding method to investigate the core-shell structure of the catalyst. SEM images were measured on a Nova NanoSEM 450 microscope. The average CuO NPs size was estimated by random statistical calculation.

The textural properties of the samples were evaluated by N_2 adsorption–desorption isotherms at −196 °C using a physisorption analyzer (Micromeritics ASAP 2020). Prior to the analysis, the sample was degassed at 300 °C for 6 h to remove any moisture and impurities. The surface area was calculated using the Brunauer–Emmett–Teller (BET) model for adsorption data obtained in a relative pressure range of 0.05–0.30. The pore size distribution was determined from the amount of N_2 adsorbed at a relative pressure of 0.99 using the Barrett–Joyner–Halenda (BJH) algorithm. The average pore diameter of samples was determined by a desorption branch according to the Barrett–Joyner–Halenda (BJH) model.

In situ diffusion reflectance infrared Fourier transform spectra of CO adsorption (CO-DRIFTS) were recorded using a Fourier transform infrared spectrometer (PerkinElmer, Frontier) with a mercury cadmium telluride (MCT-A) detector and an in situ cell (modified Harricks Model HV-DR2), with a resolution of 4 cm^{-1}. Before adsorption, the sample was reduced on line following the same method used in reactions and then cooled to 15 °C in Ar. All infrared data were evaluated in Kubelka-Munk units, which are linearly related to the absorber concentration in spectra.

UV-Vis DRS spectra were collected using a Lambda 750 UV–vis-NIR spectrometer equipped with a diffuse reflectance spectroscopy (DRS) accessory. The spectra were collected between 200 and 900 nm with an interval of 1 nm using $BaSO_4$ as a reference and were transformed into the Kubelka–Munk function, F(R).

XPS analysis was carried out on a Thermo Fisher Scientific ESCALAB 250Xi spectrometer with Al-Kα radiation (hν = 1486.6 eV, pass energy: 40.0 eV) as the X-ray source. To compensate for surface charge effects, all the binding energies (BEs) were calibrated using the C1s line at 284.80 eV.

The X-ray absorption near-edge structure (XANES) spectra of the Cu K edge were measured at the BL14W1 beamline, Shanghai Synchrotron Radiation Facility (SSRF), with electron beam energy of 3.5 GeV under “top-up” mode (current: 220 mA). The samples were measured at room temperature using a fixed-exit monochromator equipped with two flat Si(111) crystals. Data on the catalysts and reference samples (Cu foil, Cu_2O powder and CuO powder) were collected in the transmission mode (Oxford ion chamber). Athena and Artemis software were used to extract the data and to fit the curves, respectively.

2.3. Catalytic performance test

The catalytic activity of Cu@SiO_2 catalysts was evaluated for the degradation of rhodamine B (RhB). A typical reaction was performed in a batch reactor containing 100 mL of 10 ppm RhB, 0.5 g/L catalyst and 1000 ppm H_2O_2 while the suspension was stirred at 60 °C. At the given reaction time intervals, 3 mL supernatant solution was collected by filtration through a 0.22 μm Nafion membrane for the analysis of RhB concentration and the leaching amount of metal ions. The concentration of RhB was determined at its maximum absorption wavelength of 554 nm using an UV–vis spectrophotometer. The copper leaching was measured by ICP-MS. The concentration of ·OH was measured indirectly using benzoic acid as a probe molecule.

2.4. DFT calculations

Spin-polarized DFT calculations were performed using the Vienna ab-initio simulation package (VASP) [27,28]. A plane-wave basis set with a cut-off energy of 450 eV was used to expand the Kohn–Sham wave functions. The interactions between the ionic cores and valence electrons were described using a projector augmented wave (PAW) method [29,30], and the exchange-correlation effects were self-consistently described within the Perdew–Burke–Ernzerh of generalized gradient approximation (GGA-PBE) [31,32]. The occupation of electronic states was determined using the method Gaussian smearing

method [33] and the smearing width was 0.01 eV. Optimized geometries were obtained by minimizing the root mean square (rms) forces on the atoms until they are smaller than 0.05 eV/Å.

Cu(111), Cu_2O(111) and Cu(111) slab models were built to simulate Cu catalysts with active species of Cu^0, Cu^+ and Cu^{2+}, respectively. Cu (111) was modeled as a four-atomic-layer slab with (3 × 3) unit cell. Cu_2O(111) and CuO(111) were modeled as four-atomic-layer slabs with (1 × 1) and (2 × 1) unit cells, respectively. The topmost two layers of the three models were relaxed. A vacuum spacing of 12 Å along the normal direction (z) to the surface and a 3 × 3×1 Monk horst-Pack k-point mesh were used for all the models.

The binding energy (BE) of surface species was calculated by Eq. 1:

$$BE = E_{adsorbate/surface} - E_{clean} - E_{adsorbate} \quad (1)$$

where $E_{adsorbate/surface}$, E_{clean} and $E_{adsorbate}$ are the total energies of the Cu(111), Cu_2O(111) and CuO(111) models with the adsorbate on it, the clean models without the adsorbed species, and the neutral adsorbate species in the gas phase, respectively.

3. Results and discussion

3.1. Catalytic performance test

The catalytic performance of $Cu@SiO_2$ with different reduction temperatures was tested for the oxidative degradation of RhB, which is a typical organic contaminant from the dyeing industry and has long been used as a reference organic contaminate [21,34–36].

To explore the adsorption effects of RhB, the adsorption experiments were performed in a H_2O_2-free solution. As shown in Fig. 1(a), less than 10% of RhB was adsorbed by $Cu@SiO_2$, indicating that the conversion due to the adsorption could be negligible. The catalytic degradation efficiency of $Cu@SiO_2$ catalysts were also illustrated in Fig. 1(a). For the unreduced $Cu@SiO_2$ catalyst, only 23.4% RhB was degraded in 10 min. However, more than 95% removal was achieved using $Cu@SiO_2$-R200 in 10 min. It is noteworthy that the heterogeneous Fenton catalytic system for $Cu@SiO_2$-R200 also has a higher RhB degradation efficiency than reported systems, as presented in Table S1 [21,34–36]. With further increasing the reduction temperature, the degradation rate declined. Approximate 76% RhB removal was obtained over $Cu@SiO_2$-R450 in 10 min. These catalytic degradation results indicate that the reduction temperature in preparation significantly affects the performance of Cu catalysts. Due to the strong oxidative property of H_2O_2, the control experiment was conducted in absent of catalyst, and only about 15% of RhB was degraded after 10 min reaction. This confirms that the interaction between H_2O_2 and the catalyst led to the efficient decomposition of RhB. The concentration of leaching Cu ions of $Cu@SiO_2$, $Cu@SiO_2$-R200 and $Cu@SiO_2$-R450 was 0.03, 0.07 and 0.17 ppm 0.03 ppm, respectively, which was much lower than the legal limit (2 ppm) enforced by the directives of the European Union.

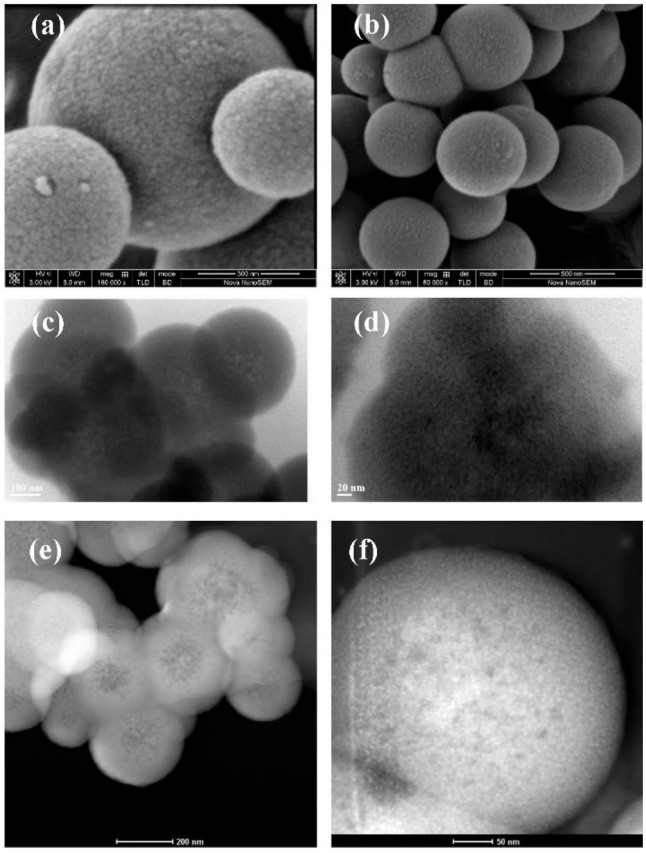

Fig. 2. (a)–(b) SEM, (c)–(d) TEM and (e)–(f) HADDF-STEM images of as-prepared $Cu@SiO_2$ catalysts.

Furthermore, experiments in the homogeneous Fenton system was also carried out to compare the activities of homogeneous and heterogeneous Fenton catalysis for RhB degradation. The reaction rate for $Cu@SiO_2$-R200 was close to that of the homogeneous catalysis system. Therefore, the heterogeneous Fenton system with $Cu@SiO_2$-R200 can achieve comparable performance as the homogeneous Fenton system without generating heavy-metal pollution of copper ions.

For the kinetics study, the pseudo-first order model was used to predict the reaction kinetics (Eq. 2). The kinetics parameters were comparatively studied with different reaction conditions and copper

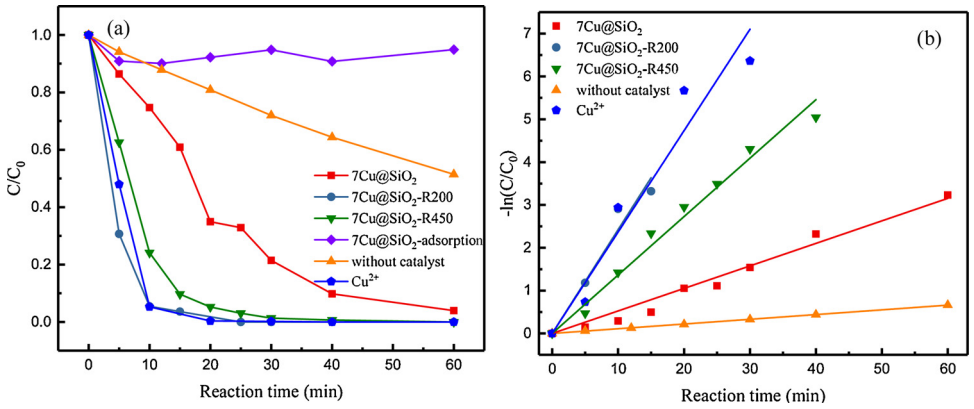

Fig. 1. (a) RhB removal efficiency in different catalytic systems. (b) Corresponding responses of $\ln(C/C_0)$ to the reaction time fitted based on the pseudo-first-order kinetics. (Reaction conditions: 60 °C, 1000 ppm H_2O_2, 0.035 g/L Cu, 10 ppm RhB.).

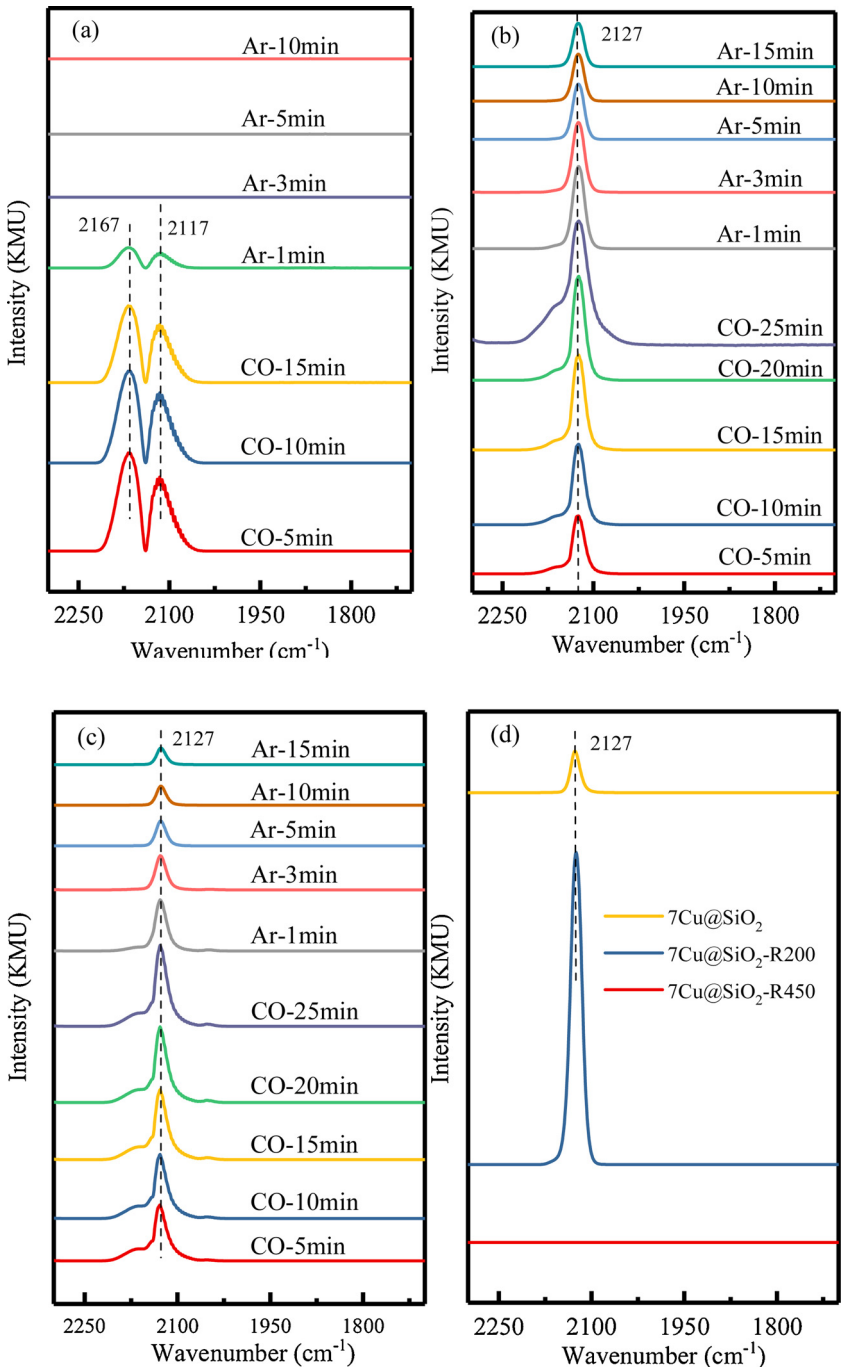

Fig. 3. In situ DRIFTS spectra of CO adsorption over the synthesized samples in an Ar flow. (a) Cu@SiO_2, (b) Cu@SiO_2-R200, (c) Cu@SiO_2-R450, (d) Comparison of intensity of DRIFTS spectra on Cu@SiO_2, Cu@SiO_2-R200 and Cu@SiO_2-R450 catalysts.

catalysts.

$$-\ln(C/C_0) = k_{app}t \quad (2)$$

Where C_0 (ppm) and C (ppm) are the concentrations of RhB at the initial reaction time and time t (min), respectively, and k (min^{-1}) is the pseudo-first-order reaction rate constant. The linear plots of $-\ln(C/C_0)$ vs. t of the pseudo-first order model was showed in Fig. 1(b), implying that RhB degradation over these catalysts can be described using first-order reaction kinetics. The calculated reaction rate constants k_{app} were 0.040, 0.242 and 0.136 min^{-1} for Cu@SiO_2, Cu@SiO_2-R200 and Cu@SiO_2-R450 (Table S2), respectively, indicating that the reduction pretreatment improved the catalytic activity by 2.6–6.1 times.

3.2. Morphology and crystal structure

The morphology of the fresh Cu@SiO_2 catalysts were characterized by SEM and TEM. As shown in Fig. 2, Cu@SiO_2 catalysts exhibit a uniform spherical shape with a diameter of 350–600 nm. TEM images revealed a core-shell structure, with CuO NPs (2–3 nm) as the core, encapsulated by a silica shell. XRD patterns of all prepared samples showed broad characteristic diffraction peaks of amorphous silica around 23°. No obvious diffraction peaks of CuO (Fig. S1) were observed, indicating that the size of CuO was less than 5 nm, which agreed with TEM results. Instead, peaks at 35.6°, 38.8° and 48.8° corresponding to CuO can be detected for the catalysts prepared by an impregnation method (Cu/SiO_2), manifesting that the dispersion of Cu species in Cu@

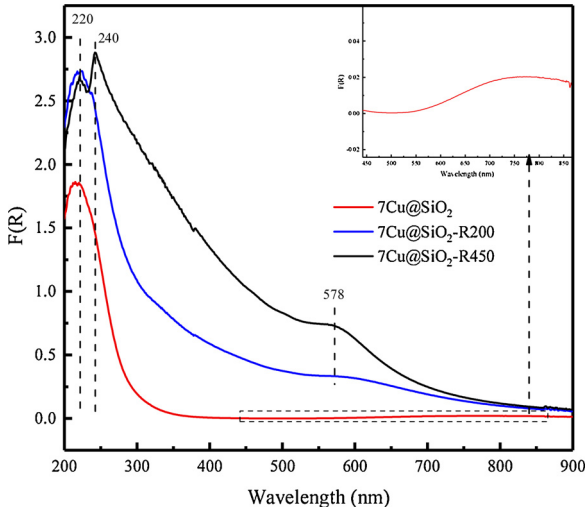

Fig. 4. UV-DRS spectra of various catalysts.

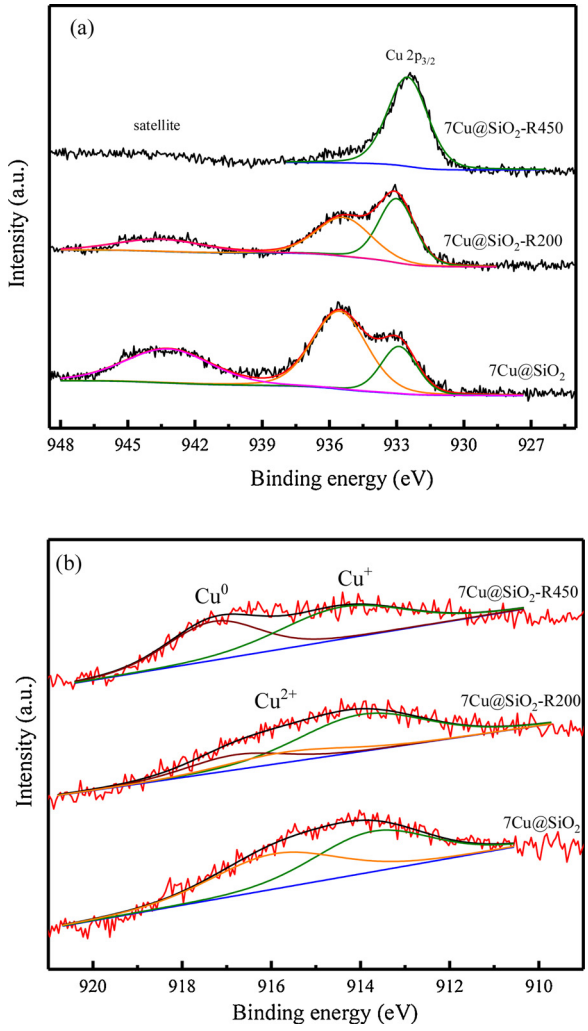

Fig. 5. XPS spectra of as prepared samples, (a) Cu 2p, (b) Cu LMM.

SiO_2 is higher than that in Cu/SiO_2. The XRD results also confirmed that the other two catalysts thermally reduced at 200 and 450 °C showed no characteristic peaks of copper species, indicating reduction temperature range (200–550 °C) did not affect the dispersity of Cu species dramatically.

From TEM and HADDF-STEM, it can be seen that only a small portion of CuO NPs dispersed on the surface of SiO_2 shell, and most of CuO NPs distributed in the core (Fig. S2). The BET specific surface area of as-prepared $Cu@SiO_2$ is 48 m^2/g with an average pore diameter of 3.3 nm. Moreover, we included the N_2 adsorption-desorption isotherms and pore size distributions of $Cu@SiO_2$ into SI (Fig. S3).

3.3. Electronic structure

In order to determine the structure-performance relationship of these $Cu@SiO_2$ catalysts, the chemical states of the surface Cu species were analyzed by in situ CO-DRIFTS (Fig. 3(a)), where CO is used as a probe molecule. The first doublet peak located at 2115–2170 cm^{-1} corresponded to the signal of gaseous CO [37]. The peak intensity decreased gradually in an Ar flow at 15 °C and completely diminished after flushing for only 3 min. These results suggested that the adsorption of CO on Cu species was very weak, because the interaction between Cu^{2+} and CO is mainly electrostatic, which does not allow the formation of stable Cu^{2+}—CO bond [38].

The spectra of CO adsorbed on $Cu@SiO_2$-R200 and $Cu@SiO_2$-R450 were shown in Fig. 3(b) and (c), respectively. It can be seen that only one peak locates at 2127 cm^{-1} was detected in all three copper catalysts. However, there is still controversy on the peak assignment at 2127 cm^{-1}. Knözinger et al. referred that Cu^+ forms strong bonds with CO via σ- and π-back bonding contributions due to its low charge and high d-electron density [38], and CO adsorption on oxide-supported Cu^+ is characterized by bands around 2120–2140 cm^{-1} [39]. In addition, Vannice et al. proposed that the adsorption of CO on Cu^0 sites was weak and reversible at room temperature; CO binds most strongly on Cu^+ sites, which could be detected at 2110–2135 cm^{-1} [40]. In contrast, Spivey et al. found that a completely reduced Cu/SiO_2 catalyst showed an absorption peak at 2127 cm^{-1}, which were ascribed as Cu^0—CO [41,42].

To further verify the Cu species where CO adsorption occurred, the CO-DRIFTS of Cu^0 powder was carried out. It is well known that the Cu^0 with small particle size is easily oxidized once exposed to air. To avoid the oxidation of metallic Cu powder, the samples was first reduced at 450 °C for 2 h on line to remove all the oxide species on the surface [43,44] before being subjected to CO-DRIFTS experiments (Fig. S4). After the Ar purge, the IR-band at 2127 cm^{-1} was not observed, indicating the band at 2127 cm^{-1} can only be ascribed to Cu^+—CO sites. In addition, it can be observed from Fig. 3(d) that peak intensity of Cu^+—CO was obviously decreased as reduction temperature increased from 200 °C to 450 °C, and it indicates that the Cu^+ fraction on the catalyst surface decreased.

The electronic structure was further characterized by UV–vis DRS (Fig. 4). The spectrum of the samples exhibited two strong peaks at 220 and 240 nm, which could be assigned to the charge-transfer transitions of the ligand O_2 to an isolated metal center Cu^{2+} (Si—O—Cu), and small CuO clusters [45], respectively. The broad and weak absorption band in the region of 600–800 nm was owing to the d–d transition of Cu^{2+} in the pseudo-octahedral ligand field generated by oxygen ions, indicating the presence of larger CuO particles [7]. However, all $Cu@SiO_2$ samples showed no such peaks in the range of 600–800 nm, indicating that the majority of Cu species in these catalysts are evenly distributed on the support. Although the complexes of Cu^+ (d10) have no d–d transition, Cu_2O can give transitions from the valence band to excitation levels involving the emission and absorption of a photon [46]. Upon the reduction of $Cu@SiO_2$ at 200 °C, an absorption edge at 578 nm attributed to metallic Cu appeared, and the intensity of which increased when the reduction temperature rose to 200 °C and 450 °C [46].

The XPS results of Cu 2p and Auger Cu LMM were shown in Fig. 5, the deconvolution of the asymmetrical Cu $2p_{3/2}$ signals of $Cu@SiO_2$ and $Cu@SiO_2$-R200 revealed the presence of different Cu species. The observed Cu $2p_{3/2}$ peaks at binding energy (BE) of 935.5 eV and the shake-up peak at 939–948 eV demonstrated the existence of Cu^{2+}, while the

Table 1
XPS parameters and the Cu^+ fraction of various catalysts.

Sample	XPS parameters				
	Cu $2p_{3/2}$ ((Cu^0+Cu^+)/Cu^{2+}, eV)	Cu Auger (Cu^0/Cu^+/Cu^{2+}, eV)	Cu^+/Cu^{2+}	Cu^+/Cu^0	Cu^+ fraction
$Cu@SiO_2$	932.9/935.5	-/913.7/915.9	0.40	–	0.29
$Cu@SiO_2$-R200	933.0/935.4	916.8/913.9/915.7	3.79	3.24	0.64
$Cu@SiO_2$-R450	932.5/-	917.2/914.4/-	–	0.75	0.43

Table 2
Ratio of atomic concentrations of elements calculated from XPS data on various catalysts.

sample	Atomic concentration (%)			
	Cu	Si	O	C
$Cu@SiO_2$	1.34	29.59	64.73	4.34
$Cu@SiO_2$-R200	1.53	27.05	59.92	11.50
$Cu@SiO_2$-R450	0.87	28.93	60.08	10.12

Cu $2p_{3/2}$ peaks at a lower BE of 932.9 eV and absence of the shake-up peak were the characteristic features of reduced Cu species [47–49]. Only one distinct Cu $2p_{3/2}$ peak at 932.9 eV was observed for $Cu@SiO_2$-R450, demonstrating that the surface Cu^{2+} was fully reduced. The presence of Cu^+ was distinguished by the peak at kinetic energy (KE) of 913.7 eV in Cu LMM lines. By the deconvolution of the Cu LMM peak, two peaks at 914.7 and 917.2 eV revealed the existence of both Cu^+ and Cu^0 on the $Cu@SiO_2$-R450 surface [26,50].

Obviously, the peak intensity of Cu^+ significantly increased after reduction with H_2. The Cu^+ fraction obviously increased from 0.29 ($Cu@SiO_2$) to 0.64 ($Cu@SiO_2$-R200), however, with further increasing the reduction temperature, part of Cu^+ transferred into Cu^0, and the Cu^+ fraction slightly dropped to 0.43 ($Cu@SiO_2$-R450). Thus, proper reduction facilitates the generation of Cu^+ and improves the catalytic activity remarkably (Table 1).

In addition, XPS analysis (Table 2) showed that surface Cu concentrations were much lower than the nominal loadings, suggesting that Cu species were dispersed inside the SiO_2 sphere, being consistent with the results of TEM and HADDF-STEM.

Furthermore, XANES was also employed to determine the valence of Cu species embedded inside the pores of catalysts [51]. Fig. 6(a) and (b) showed Cu K-edge XANES spectra and their first derivative profiles of different catalysts. The energy of absorption edge (E_0) of Cu species increases with raising oxidation degree, and the E_0 at 8978.9, 8980.3 and 8982.9 eV are characteristics of Cu foil, Cu_2O and CuO, respectively. Notably, the intensity of the peak at 8985.8 eV corresponding to Cu^{2+} in $Cu@SiO_2$ decreased after H_2 reduction, while the peak intensity of Cu^0 and Cu^+ significantly increased. Moreover, the intensity of Cu^+ peak became lower than that of Cu^0 when the reduction temperature rose from 200 to 450 °C. This indicates that Cu^{2+} was first reduced to Cu^+, and then Cu^+ was reduced to Cu^0 with the reduction temperature increase. Besides, it can be observed that the peak ascribed to Cu^{2+} of $Cu@SiO_2$ shifted to a higher energy of 8985.8 eV, while the corresponding peak of Cu/SiO_2 kept the same absorption edge energy as CuO. The energy positions of the dipole-forbidden 1s→3d electronic transition peak (pre-edge peak) in the Cu K-edge XANES spectra were strongly influenced by the chemical states of Cu^{2+}, which were determined by the coordination geometries (tetrahedral, octahedral and square planar) and ligand electronegativity [51], so the shift of Cu^{2+} peak shows that there is an increase in the ligand field strength [52], being consistent with the results of UV–vis DRS.

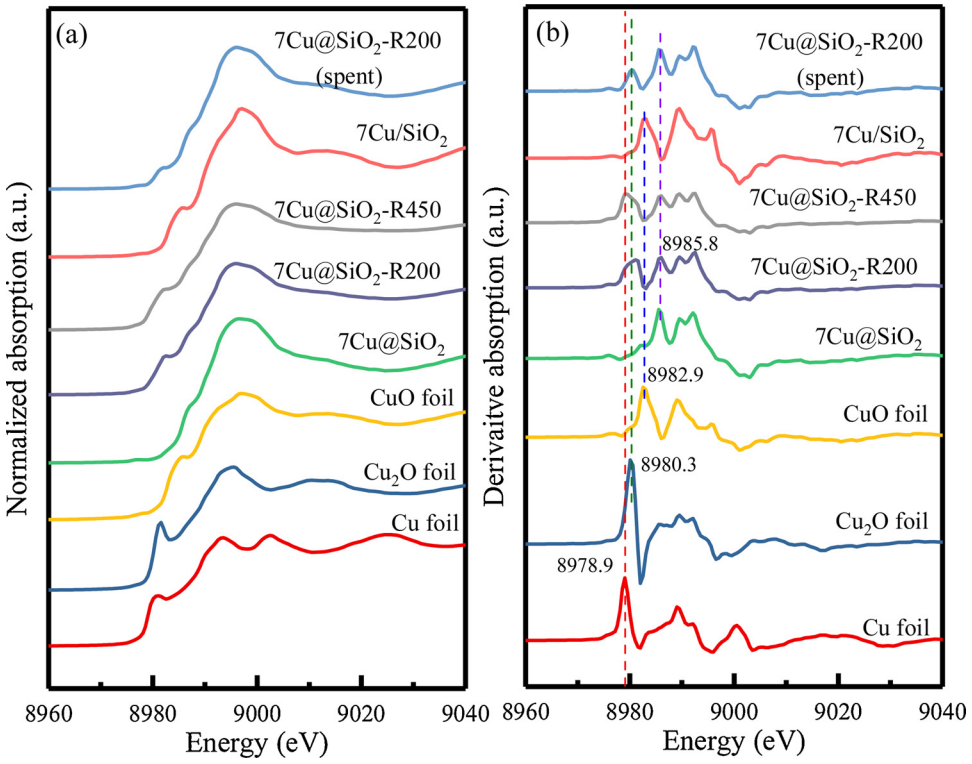

Fig. 6. (a) Cu K-edge XANES curves of as-prepared Cu based and reference catalysts and (b) corresponding first derivative profiles.

Table 3
XANES parameters and the calculated LCF results of various catalysts.

Sample	Pre-edge position (eV)			Cu^0 fraction	Cu^+ fraction	Cu^{2+} fraction
	Cu^0	Cu^+	Cu^{2+}			
Cu foil	8978.9	–	–	1.00	–	–
Cu_2O foil	–	8980.3	–	–	1.00	–
CuO foil	–	–	8982.9	–	–	1.00
$Cu@SiO_2$	–	–	8985.8	–	–	1.00
$Cu@SiO_2$-R200	8978.9	8980.3	8985.8	0.28	0.28	0.44
$Cu@SiO_2$-R450	8978.9	8980.3	8985.8	0.43	0.21	0.36
Cu/SiO_2	0	0	8982.9	–	–	1.00

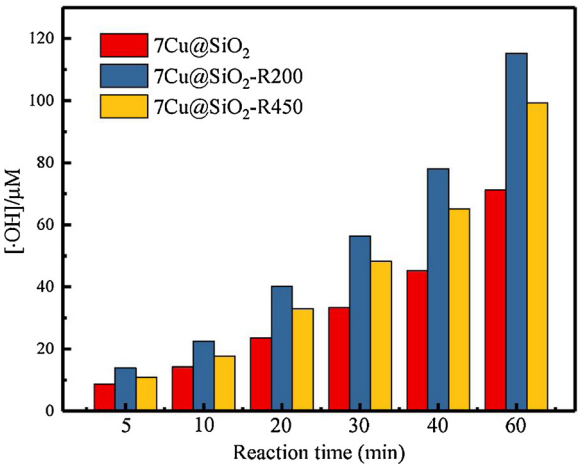

Fig. 7. The concentration of generated ·OH using different catalysts. (Reaction conditions: 60 °C, 1000 ppm H_2O_2 (30%), 0.5 g/L catalyst, 1500 ppm benzoic acid.).

After analyzing the linear combination fitting (LCF) results of first derivative profiles of reduced catalysts, the contents of different Cu species of $Cu@SiO_2$-R200 and $Cu@SiO_2$-R450 were listed in Table 3. With the increase in reduction temperature from 200 to 450 °C, the Cu^0 fraction increased from 0.28 to 0.43, whilst the Cu^{2+} and Cu^+ fraction decreased from 0.44 and 0.28 to 0.36 and 0.21, respectively, indicating that the reduction of Cu^+ was accelerated by increasing reduction temperature.

3.4. The structure-performance relationship

The characterization results of CO-DRIFTS, UV–vis DRS, XPS and XANES suggested that Cu^+ was produced by reducing $Cu@SiO_2$ with H_2 and reached its maximum after reduction at 200 °C; further increasing reduction temperature resulted in the rise of Cu^0 content. The similar results have also been observed by Yang et al [26]. Moreover, the degradation activity of $Cu@SiO_2$-R200 also is the highest compared with the catalysts reduced in other temperatures. Accordingly, we hypothesized that all these Cu species (Cu^{2+}, Cu^+, and Cu^0) could activate H_2O_2 and produce ·OH, while the Cu^+ was the primary active species. We believe that it is the reason for the highest catalytic performance of $Cu@SiO_2$-R200 among those catalysts.

In order to verify our hypothesis, the qualitative and quantitative determination of ·OH was carried out. It is widely recognized that the H_2O_2 activation and the generation of ·OH radicals play a vital role in the advanced oxidation of organic pollutants [53,54]. To demonstrate the generation of ·OH, 5-tert-Butoxycarbonyl-5-methyl-1-pyrroline-N-oxide (BMPO) spin trapped electron paramagnetic resonance (ESR) was performed. As shown in Fig. S5, the influence of H_2O_2 was excluded because no peak could be observed in the solution without catalyst. After adding $Cu@SiO_2$, four characteristic peaks of BMPO-·OH were observed, manifesting the generation of ·OH.

In addition, the number of generated ·OH radicals is a crucial parameter for evaluating the activity of catalyst. To quantitively analysis of ·OH radicals, a probing molecule such as benzoic acid is usually used [20,53]. According to the previous work, the rate constant of the reaction between benzoic acid and ·OH in aqueous media is 4.2×10^9 M^{-1} s^{-1}, and 1 mol p-hydroxybenzoic acid (p-HBA) is produced quantitatively by consuming 5.87 ± 0.18 mol ·OH [55–57]. The obtained results were presented in Fig. 7. The ·OH concentration generated by catalysts gradually increased with reaction time. The maximal value (115.3 μM) was obtained for $Cu@SiO_2$-R200, much higher than that obtained with other Cu/SiO_2 catalysts [58]. It also can be seen that $Cu@SiO_2$ and $Cu@SiO_2$-R450 produced 71.1 μM and 99.3 μM ·OH, respectively, and the ratio of ·OH amount produced by $Cu@SiO_2$-R200 and $Cu@SiO_2$-R450 is 1.2, which is coincided with the Cu^+ fraction ratio calculated on the basis of XANES characterization results. Therefore, it can be deduced that Cu^+ is the most active species of Cu catalysts.

In order to get deep insight into the catalytic roles of different Cu species, Cu(111), Cu_2O(111) and CuO(111) models were built to simulate Cu^0, Cu^+ and Cu^{2+}, respectively; meanwhile, their catalytic performance for H_2O_2 activation was simulated using the DFT method. Facile adsorption of H_2O_2 is critical for ·OH generation on Cu-based catalysts. We thus adopted the BE of H_2O_2 on the Cu models as descriptor to estimate the performance of different Cu species. The results showed that Cu_2O(111) possesses moderate capacity for the adsorption of H_2O_2 on Cu_2O(111) (BE = −1.12 eV), while the binding strength of H_2O_2 on Cu(111) (BE = −0.18 eV) and CuO(111) (BE = −0.42 eV) is much weaker, indicating that Cu^+ possesses the highest capacity for the activation of H_2O_2 (Fig. 8). Accordingly, Cu^+ species is most active for H_2O_2 activation and ·OH generation, followed by Cu^{2+} and Cu^0.

Considering that the Cu leaching was quite low (less than 0.2 ppm), the impact of the homogeneous Cu^{2+} ion could be excluded. Therefore, we suggest that the generation of ·OH free radicals over the heterogeneous copper catalysts, which takes place on the catalyst surface, primarily follows the catalytic decomposition mechanism (Eqs. 3–5) [59,60].

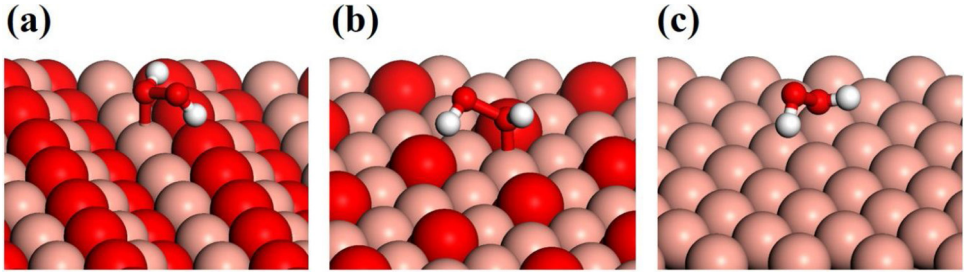

Fig. 8. The adsorption of H_2O_2 on CuO(111) (a), Cu_2O(111) (b), and Cu(111) (c) surfaces. Brick red, red and white spheres are copper, oxygen and hydrogen atoms, respectively (For interpretation of the references to colour in this figure legend, the reader is referred to the web version of this article).

Table 4
Degradation of various contaminants.

Entry	Contaminants	Initial conc. (ppm)	Conv. (30 min) (%)	Conv. (60 min) (%)
1	Methyl blue (MB)	10	97.8	100
2	Methyl orange (MO)	10	99.8	100
3	4-chlorophenol (4CP)	40	100.0	100
4	Nitrobenzene (NB)	100	61.6	75.7
5	Quinoline	50	44.89	68.6

*The initial H_2O_2 concentration is 1000 ppm.

$H_2O_2(ads) \rightarrow 2{\cdot}OH$ (Eq. 3)

$\cdot OH\ (ads) + H_2O_2(ads) \rightarrow H_2O(ads) + \cdot OOH(ads)$ (Eq. 4)

$2{\cdot}OOH \rightarrow H_2O_2(ads) + O_2$ (Eq. 5)

Cu^+ possesses the highest capacity for ·OH generation and the subsequent degradation reactions, and it thus acts as the primary active species for this reaction system. Therefore, the Cu@SiO_2 without reduction pretreatment only contains Cu^{2+} species showed the poorest activity for ·OH generation and RhB degradation (Fig. 1 and Fig. 7). The reduction of Cu@SiO_2 at 200 °C results in the highest portion of Cu^+ species in the catalyst, thus exhibiting the highest catalytic activity in the degradation reaction. Further increasing reduction temperature to 450 °C leads to the decline of the Cu^+ content, and the activity also drops. As a result, by varying reduction temperature, the active species of Cu catalysts can be finely tuned and pollutants can be decomposed efficiently.

3.5. Adaptability and reusability of Cu@SiO_2-R200

To investigate the adaptability of Cu@SiO_2-R200 in removing various pollutants, degradation experiments of selected model pollutants, such as chemical dyes, phenols, and nitrogen-containing compounds, were performed for the Cu@SiO_2-R200 at neutral pH. As listed in Table 4, all refractory compounds were substantially degraded at 30 min, especially 4CP (40 ppm), MO (10 ppm) and MB (10 ppm), which could be completely removed in 30 min. Even for the extremely refractory N-containing pollutants, nitrobenzene and quinoline, the conversion could reach 75.7% and 68.6%, respectively, within 60 min. These experimental results suggested that Cu@SiO_2-R200 was applicable to degrade various organic pollutants efficiently.

From the perspective of practical application, the reusability of the catalysts is of great importance. As a result, the recyclability of Cu@SiO_2-R200 was evaluated by reducing the spent catalysts in H_2 at 200 °C and subjecting to the next degradation reaction cycle. The RhB removal efficiency was recorded after 60 min. The results showed that the catalyst can be recycled for 4 times without significant activity loss (Fig. S8) (Fig. 9).

4. Conclusions

In this work, plum pudding-like core shell structure Cu@SiO_2 with high dispersion was fabricated and tested for the degradation of organic pollutants. Cu atoms were co-incorporated into the framework of SiO_2 by chemical bonding of Si-O-Cu, which is confirmed by HAADF, XRD and UV–vis DRS. The RhB degradation is markedly affected by reduction temperature and Cu@SiO_2-R200 exhibited excellent performance for degradation and mineralization of the refractory organic pollutants in the presence of H_2O_2 under neutral pH conditions. CO-DRIFTS, UV–vis DRS, XPS and XANES spectra indicated that Cu^+ can be generated both on the surface and in the bulk phase of catalysts, being the most active species for the generation of ·OH. Most of the refractory compounds were substantially degraded over Cu@SiO_2-R200 at 30 min. Even for the extremely refractory N-containing pollutants, nitrobenzene and quinoline, the conversion could reach 75.7% and 68.6%, respectively, within 60 min.

Combining the experiment results with DFT calculations, we have identified that Cu^+ acts as the primary active species of Cu-based heterogeneous Fenton catalysts for H_2O_2 activation and ·OH generation. Cu^+ species, as high-energy species, is more reactive than Cu^0 and Cu^{2+} species for Fenton reaction. Therefore, the synthesis of highly stable catalysts with high ratio of Cu^+ species is crucial for the development of heterogeneous Fenton catalysts.

Acknowledgements

The authors are grateful to the support from the National Science Foundation (21808057), Fundamental Research Funds for the Central Universities (222201718002), China Postdoctoral Science Foundation (2018M641941 and 2019T120313) and Innovation Scientists and Technicians Troop Construction Projects of Henan Province. The authors thank Research Center of Analysis and Test of East China University of Science and Technology for the help on TEM analysis. The authors thank beamline BL14W1 (Shanghai Synchrotron Radiation Facility) for providing the beam time.

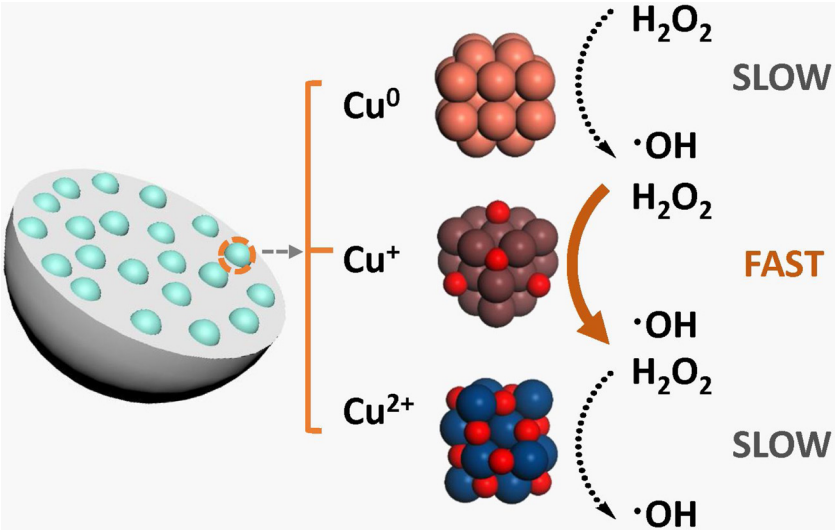

Fig. 9. Mechanism of ·OH generation over Cu species with different chemical states in the presence of H_2O_2.

Appendix A. Supplementary data

Supplementary material related to this article can be found, in the online version, at doi:https://doi.org/10.1016/j.apcatb.2019.117985.

References

[1] X.-j. Yang, X.-m. Xu, J. Xu, Y.-f. Han, Iron Oxychloride (FeOCl): an efficient Fenton-like catalyst for producing hydroxyl radicals in degradation of organic contaminants, J. Am. Chem. Soc. 135 (2013) 16058–16061.

[2] Y. Sheng, Y. Sun, J. Xu, J. Zhang, Y.-F. Han, Fenton-like degradation of rhodamine B over highly durable Cu-embedded alumina: kinetics and mechanism, AlChE J. 64 (2018) 538–549.

[3] M.A. Oturan, J.-J. Aaron, Advanced oxidation processes in water/wastewater treatment: principles and applications. A review, Crit. Rev. Environ. Sci. Technol. 44 (2014) 2577–2641.

[4] J.L. Wang, L.J. Xu, Advanced oxidation processes for wastewater treatment: formation of hydroxyl radical and application, Crit. Rev. Environ. Sci. Technol. 42 (2012) 251–325.

[5] L. Lyu, L. Zhang, Q. Wang, Y. Nie, C. Hu, Enhanced Fenton catalytic efficiency of γ-Cu-Al_2O_3 by σ-Cu^{2+}-ligand complexes from aromatic pollutant degradation, Environ. Sci. Technol. 49 (2015) 8639–8647.

[6] L. Lyu, L. Zhang, C. Hu, Enhanced Fenton-like degradation of pharmaceuticals over framework copper species in copper-doped mesoporous silica microspheres, Chem. Eng. J. 274 (2015) 298–306.

[7] L. Lyu, L. Zhang, C. Hu, M. Yang, Enhanced Fenton-catalytic efficiency by highly accessible active sites on dandelion-like copper-aluminum-silica nanospheres for water purification, J. Mater. Chem. A 4 (2016) 8610–8619.

[8] F.L.Y. Lam, A.C.K. Yip, X. Hu, Copper/MCM-41 as a highly stable and pH-insensitive heterogeneous photo-Fenton-like catalytic material for the abatement of organic wastewater, Ind. Eng. Chem. Res. 46 (2007) 3328–3333.

[9] T. Granato, A. Katovic, K.M. Valkaj, A. Tagarelli, G. Giordano, Cu-silicalite-1 catalyst for the wet hydrogen peroxide oxidation of phenol, J. Porous Mater. 16 (2009) 227–232.

[10] N. Helaïli, Y. Bessekhouad, A. Bouguelia, M. Trari, Visible light degradation of Orange II using xCu_yO_z/TiO_2 heterojunctions, J. Hazard. Mater. 168 (2009) 484–492.

[11] J.K. Kim, I.S. Metcalfe, Investigation of the generation of hydroxyl radicals and their oxidative role in the presence of heterogeneous copper catalysts, Chemosphere 69 (2007) 689–696.

[12] G. Wen, S.-J. Wang, J. Ma, T.-L. Huang, Z.-Q. Liu, L. Zhao, J.-L. Xu, Oxidative degradation of organic pollutants in aqueous solution using zero valent copper under aerobic atmosphere condition, J. Hazard. Mater. 275 (2014) 193–199.

[13] P. Zhou, J. Zhang, Y. Zhang, J. Liang, Y. Liu, B. Liu, W. Zhang, Activation of hydrogen peroxide during the corrosion of nanoscale zero valent copper in acidic solution, J. Mol. Catal. A Chem. 424 (2016) 115–120.

[14] Y. Sun, Z. Yang, P. Tian, Y. Sheng, J. Xu, Y.-F. Han, Oxidative degradation of nitrobenzene by a Fenton-like reaction with Fe-Cu bimetallic catalysts, Appl. Catal. B-Environ. 244 (2019) 1–10.

[15] M.H. Robbins, R.S. Drago, Activation of hydrogen peroxide for oxidation by copper (II) complexes, J. Catal. 170 (1997) 295–303.

[16] L.G. Covinich, P. Massa, R.J. Fenoglio, M.C. Area, Oxidation of hazardous compounds by heterogeneous catalysis based on Cu/Al_2O_3 system in Fenton-type reactions, Crit. Rev. Environ. Sci. Technol. 46 (2016) 1745–1781.

[17] P. Massa, F. Ivorra, P. Haure, R. Fenoglio, Preparation and characterization of wet-proofed CuO/Al_2O_3 catalysts for the oxidation of phenol solutions, Catal. Lett. 101 (2005) 201–209.

[18] V. Subbaramaiah, V.C. Srivastava, I.D. Mall, Catalytic activity of Cu/SBA-15 for peroxidation of pyridine bearing wastewater at atmospheric condition, AlChE J. 59 (2013) 2577–2586.

[19] S. Lan, Y. Xiong, S. Tian, J. Feng, T. Xie, Enhanced self-catalytic degradation of CuEDTA in the presence of H_2O_2/UV: evidence and importance of Cu-peroxide as a photo-active intermediate, Appl. Catal. B-Environ. 183 (2016) 371–376.

[20] T.-Y. Lin, C.-H. Wu, Activation of hydrogen peroxide in copper(II)/amino acid/H_2O_2 systems: effects of pH and copper speciation, J. Catal. 232 (2005) 117–126.

[21] G. Dong, Z. Ai, L. Zhang, Total aerobic destruction of azo contaminants with nanoscale zero-valent copper at neutral pH: promotion effect of in-situ generated carbon center radicals, Water Res. 66 (2014) 22–30.

[22] R. Schlögl, Heterogeneous catalysis, Angew. Chem. Int. Ed. 54 (2015) 3465–3520.

[23] A. Paracchino, V. Laporte, K. Sivula, M. Grätzel, E. Thimsen, Highly active oxide photocathode for photoelectrochemical water reduction, Nat. Mater. 10 (2011) 456.

[24] S.H. Joo, J.Y. Park, C.-K. Tsung, Y. Yamada, P. Yang, G.A. Somorjai, Thermally stable Pt/mesoporous silica core-shell nanocatalysts for high-temperature reactions, Nat. Mater. 8 (2008) 126.

[25] Y. Yin, R.M. Rioux, C.K. Erdonmez, S. Hughes, G.A. Somorjai, A.P. Alivisatos, Formation of hollow nanocrystals through the nanoscale Kirkendall effect, Science 304 (2004) 711–714.

[26] H. Yang, Y. Chen, X. Cui, G. Wang, Y. Cen, T. Deng, W. Yan, J. Gao, S. Zhu, U. Olsbye, J. Wang, W. Fan, A highly stable copper-based catalyst for clarifying the catalytic roles of Cu^0 and Cu^+ species in methanol dehydrogenation, Angew. Chem. Int. Ed. 130 (2018) 1854–1858.

[27] G. Kresse, J. Furthmüller, Efficiency of ab-initio total energy calculations for metals and semiconductors using a plane-wave basis set, Comp. Mater. Sci. 6 (1996) 15–50.

[28] G. Kresse, J. Furthmüller, Efficient iterative schemes for ab initio total-energy calculations using a plane-wave basis set, Phys. Rev. B 54 (1996) 11169–11186.

[29] G. Kresse, D. Joubert, From ultrasoft pseudopotentials to the projector augmented-wave method, Phys. Rev. B 59 (1999) 1758–1775.

[30] P.E. Blöchl, Projector augmented-wave method, Phys. Rev. B 50 (1994) 17953–17979.

[31] J.P. Perdew, K. Burke, M. Ernzerhof, Generalized gradient approximation made simple, Phys. Rev. Lett. 77 (1996) 3865–3868.

[32] J.P. Perdew, W. Yue, Accurate and simple density functional for the electronic exchange energy: generalized gradient approximation, Phys. Rev. B 33 (1986) 8800–8802.

[33] M. Methfessel, A.T. Paxton, High-precision sampling for Brillouin-zone integration in metals, Phys. Rev. B 40 (1989) 3616–3621.

[34] L. Zhang, Y. Nie, C. Hu, J. Qu, Enhanced Fenton degradation of rhodamine B over nanoscaled Cu-doped $LaTiO_3$ perovskite, Appl. Catal. B-Environ. 125 (2012) 418–424.

[35] H. Li, J. Liao, T. Zeng, A facile synthesis of CuO nanowires and nanorods, and their catalytic activity in the oxidative degradation of rhodamine B with hydrogen peroxide, Catal. Commun. 46 (2014) 169–173.

[36] J. Fan, X. Jiang, H. Min, D. Li, X. Ran, L. Zou, Y. Sun, W. Li, J. Yang, W. Teng, Facile preparation of Cu-Mn/CeO2/SBA-15 catalysts using ceria as an auxiliary for advanced oxidation processes, J. Mater. Chem. A Mater. Energy Sustain. 2 (2014) 10654–10661.

[37] P. Tian, X. Xu, C. Ao, D. Ding, W. Li, R. Si, W. Tu, J. Xu, Y.-F. Han, Direct and selective synthesis of hydrogen peroxide over palladium-tellurium catalysts at ambient pressure, ChemSusChem 10 (2017) 3342–3346.

[38] K.I. Hadjiivanov, M.M. Kantcheva, D.G. Klissurski, IR study of CO adsorption on Cu-ZSM-5 and CuO/SiO_2 catalysts: σ and π components of the Cu^+-CO bond, J. Chem. Soc., Faraday Trans. 92 (1996) 4595–4600.

[39] K. Hadjiivanov, T. Venkov, H. Knözinger, FTIR spectroscopic study of CO adsorption on Cu/SiO_2: formation of new types of copper carbonyls, Catal. Lett. 75 (2001) 55–59.

[40] A. Dandekar, M.A. Vannice, Determination of the dispersion and surface oxidation states of supported Cu catalysts, J. Catal. 178 (1998) 621–639.

[41] M.L. Smith, A. Campos, J.J. Spivey, Reduction processes in Cu/SiO_2, Co/SiO_2, and $CuCo/SiO_2$ catalysts, Catal. Today 182 (2012) 60–66.

[42] M.L. Smith, N. Kumar, J.J. Spivey, CO Adsorption behavior of Cu/SiO_2, Co/SiO_2, and $CuCo/SiO_2$ catalysts atudied by in situ DRIFTS, J. Phys. Chem. C 116 (2012) 7931–7939.

[43] J.A. Rodriguez, J.Y. Kim, J.C. Hanson, M. Pérez, A.I. Frenkel, Reduction of CuO in H_2: in situ time-resolved XRD studies, Catal. Lett. 85 (2003) 247–254.

[44] J.Y. Kim, J.A. Rodriguez, J.C. Hanson, A.I. Frenkel, P.L. Lee, Reduction of CuO and Cu_2O with H_2: H embedding and kinetic effects in the formation of suboxides, J. Am. Chem. Soc. 125 (2003) 10684–10692.

[45] W. Su, S. Wang, P. Ying, Z. Feng, C. Li, A molecular insight into propylene epoxidation on Cu/SiO_2 catalysts using O_2 as oxidant, J. Catal. 268 (2009) 165–174.

[46] H. Praliaud, S. Mikhailenko, Z. Chajar, M. Primet, Surface and bulk properties of Cu-ZSM-5 and Cu/Al_2O_3 solids during redox treatments. Correlation with the selective reduction of nitric oxide by hydrocarbons, J. Phys. Chem. C 16 (1998) 359–374.

[47] X.-m. Zhang, P. Tian, W. Tu, Z. Zhang, J. Xu, Y.-F. Han, Tuning the dynamic interfacial structure of copper-ceria catalysts by indium oxide during CO oxidation, ACS Catal. 8 (2018) 5261–5275.

[48] T. Ghodselahi, M.A. Vesaghi, A. Shafiekhani, A. Baghizadeh, M. Lameii, XPS study of the $Cu@Cu_2O$ core-shell nanoparticles, Appl. Surf. Sci. 255 (2008) 2730–2734.

[49] S. Poulston, P.M. Parlett, P. Stone, M. Bowker, Surface oxidation and reduction of CuO and Cu_2O studied using XPS and XAES, Surf. Interface Anal. 24 (1996) 811–820.

[50] C. Xu, G. Chen, Y. Zhao, P. Liu, X. Duan, L. Gu, G. Fu, Y. Yuan, N. Zheng, Interfacing with silica boosts the catalysis of copper, Nat. Commun. 9 (2018) 3367.

[51] M.A. Fontecha-Cámara, C. Moreno-Castilla, M.V. López-Ramón, M.A. Álvarez, Mixed iron oxides as Fenton catalysts for gallic acid removal from aqueous solutions, Appl. Catal. B-Environ. 196 (2016) 207–215.

[52] K.-i. Shimizu, H. Maeshima, H. Yoshida, A. Satsuma, T. Hattori, Ligand field effect on the chemical shift in XANES spectra of Cu(II) compounds, Phys. Chem. Chem. Phys. 3 (2001) 862–866.

[53] X. Yang, P.-F. Tian, C. Zhang, Y.-q. Deng, J. Xu, J. Gong, Y.-F. Han, Au/carbon as Fenton-like catalysts for the oxidative degradation of bisphenol A, Appl. Catal. B-Environ. 134 (2013) 145–152.

[54] X.-j. Yang, P.-f. Tian, H.-l. Wang, J. Xu, Y.-f. Han, Catalytic decomposition of H_2O_2 over a Au/carbon catalyst: a dual intermediate model for the generation of hydroxyl radicals, J. Catal. 336 (2016) 126–132.

[55] S.-S. Lin, M.D. Gurol, Catalytic Decomposition of hydrogen peroxide on iron oxide: kinetics, mechanism, and implications, Environ. Sci. Technol. 32 (1998) 1417–1423.

[56] S.H. Lin, c.M. Lin, H.G. Leu, Operating characteristics and kinetic studies of surfactant wastewater treatment by Fenton oxidation, Water Res. 33 (1999) 1735–1741.

[57] M.E. Lindsey, M.A. Tarr, Quantitation of hydroxyl radical during Fenton oxidation following a single addition of iron and peroxide, Chemosphere 41 (2000) 409–417.

[58] J. Wang, C. Liu, L. Tong, J. Li, R. Luo, J. Qi, Y. Li, L. Wang, Iron-copper bimetallic nanoparticles supported on hollow mesoporous silica spheres: an effective heterogeneous Fenton catalyst for orange II degradation, RSC Adv. 5 (2015) 69593–69605.

[59] Å. Björkbacka, M. Yang, C. Gasparrini, C. Leygraf, M. Jonsson, Kinetics and mechanisms of reactions between H_2O_2 and copper and copper oxides, Dalton Trans. 44 (2015) 16045–16051.

[60] A. Hiroki, J.A. LaVerne, Decomposition of hydrogen peroxide at water-ceramic oxide interfaces, J. Phys. Chem. B 109 (2005) 3364–3370.